To be published in Applied Optics:

Title: Refractometry of organosilica microspheres

Authors: Katrina Seet, Robert Vogel, Timo Nieminen, Gregor Knöner, Halina Rubinsztein-Dunlop, Matt Trau, and Andrei Zvyagin

Accepted: 18 December 2006

Posted: 21 December 2006

Doc. ID: 74100

Refractometry of organosilica microspheres

Katrina Y T Seet[1,2], Robert Vogel[3], Timo A Nieminen[1], Gregor Knöner[1], Halina Rubinsztein-Dunlop[1], Matt Trau[3], Andrei V Zvyagin[1,2]

[1]Center for Biophotonics and Laser Science, School of Physical Sciences, The University of Queensland

[2]School of Information Technology and Electrical Engineering, The University of Queensland

[3]Nanotechnology and Biomaterials Centre, The University of Queensland, Brisbane, 4072, Australia

Phone: +61 7 3366 9727

Fax: +61 7 3365 1242

Email: seet@physics.uq.edu.au

The refractive index of novel organosilica (nano/micro)material is determined using two methods. The first method is based on analysis of optical extinction efficiency of organosilica beads versus wavelength, which is obtained by a standard laboratory spectrometer. The second method relies on the measurable trapping potential of these beads in the focused light beam (laser tweezers). Polystyrene beads were used to test these methods, and the determined dispersion curves of refractive index values have been found accurate. The refractive index of organosilica beads has been determined to range from 1.60 - 1.51 over the wavelength range of 300 - 1100 nm.

OCIS codes: 290.2200 Extinction scattering, 140.7010 Laser trapping, 290.4020 Mie theory scattering, 160.4760 Optical properties of materials

1. Introduction

Properties of (nano/micro)materials are shaped up by the bulk and structural properties of their building blocks, with an example being refractive index that determines the material's optical characteristics. These optical properties need to be precisely controlled in various applications, such as sizing of organosilica (nano/micro)beads in the flow cytometry biological assaying. By manipulating the composition of materials on the nanoscale, new structural properties have been produced. For reliable production of desirable (nano/micro)materials both bulk and structural properties need to be controlled. Since bulk properties of the material can vary as a result of nanotechnological synthesis, it is important to monitor them *in situ*. In particular, silica-derived novel material, termed organosilica, have been synthesized in the form of (nano/micro)spheres, with a range of useful qualities that have been reported.[1, 2] Organosilica surface activation have appeared to be straightforward to bind oligonucleotide and peptide sequences for optical encoding and high-throughput screening via flow cytometry.[1, 2] The optical encoding method, however, demands tight margins on organosilica microspheres size and refractive index to ensure reliable readout and correct interpretation of their scattering intensities in the context of flow cytometry. However, it has been noticed that the refractive index of organosilica microspheres is highly dependent on synthesis route[3] calling for a reliable refractometry method amenable for *in situ* implementation. Since the organosilica synthesis yields spherical particles ranging from 50 nm to 6 μm, a number of existing refractometry methods applicable for bulk materials are no longer suitable for

refractometry of this material. Among the suitable methods, an index matching method has been reported in a number of particle refractometry applications.[3, 4] In brief, particles in the solution do not scatter, i.e. rendering the sample clear, if refractive indices of the particles and solution are matched. Therefore, the solution refractive index read out at the sample maximum transmittivity provides a measure of the refractive index of the particle ensemble. Despite its conceptual simplicity, the method is tedious, requiring preparation of the new solution of predetermined refractive index per each experimental data point. The availability of suitable solutions with high refractive indices is usually limited.

The majority of existing refractometry methods for particles rely on the acquisition of optical scatter data, followed by their fitting to the theoretical model from which one can infer the particle refractive index, or its size, or both. For example, the determination of refractive index of an ensemble of microspheres have been demonstrated using holographic method of recording of the optical scatter.[5] The intensity of optical scatter has been parameterized in the Rayleigh scattering model to perform sizing of nanodiamonds.[6] Differential microscopy measurements of the optical scatter have also permitted detection of the minute cell organelle swelling, i.e. change in the scatterer's size, as a result of induced apoptosis.[7]

Scattering spectroscopy provides another approach in the determination of particle refractive index in which characteristic particle optical extinction efficiency versus wavelength is determined.[8-12] Usually, the acquired spectrum of monodisperse

microsphere samples is fitted to a theoretical model with the refractive index and microsphere size as parameters. Using this method, the refractive index for a specified wavelength range, i.e. refractive index dispersion, can be determined. The application of the scattering spectroscopy technique to refractometry of cells, bacteria, and spores has been also reported.[4, 13-15] Based on diffuse reflectance and transmittance measurements using intergrating spheres, real and imaginary refractive indices of the microspheres have demonstrated to be determined by fitting experimental data to the theoretical model, which represented a hybrid of Monte Carlo simulation and Mie theory.[16]

In this paper, we demonstrate the application of two refractometry methods to determine the refractive index of novel organosilica microspheres. Firstly, we report application of the refined scattering spectroscopy method, where we use a commercial laboratory Lamda40 spectrophotometer (Perkin Elmer) to measure the refractive index and dispersion of organosilica, following well-characterized polystyrene microsphere refractometry. Secondly, we demonstrate application of the recently reported method for measurement of the refractive index for single microparticles based on optical tweezers.[17] The two methods are compared, and a very good agreement is achieved.

2. Experimental method:

2.1 Materials

Organosilica spheres were produced using a two-step process.[2] This process involved the hydrolysis and subsequent condensation of thiol-based silica precursor. Aqueous solutions of 5.94 μm organosilica microspheres, with the addition of sodium dodecyl sulphate for the prevention of agglomeration, were prepared for spectroscopy measurements. Polystyrene microspheres (ProSciTech, 5.0% w/v in water) of mean diameters of 2.01, 2.09 and 5.26 μm, with a coefficient of variance (CV, defined as the standard deviation divided by the mean), of less than 2.4%, were diluted with MilliQ water. For the laser tweezers refractometry, 2.09 μm polystyrene and 5.16 μm organosilica microspheres were suspended in MilliQ water. Samples were prepared by placing a drop of the suspension between the microscope slide and cover slip and sealing the chamber with high viscosity silicon grease.

2.2 Methods

2.2.1 Particle Sizing

Particle sizes were measured by using a video microscopy method which was not affected by diffraction broadening. The particle under investigation was brought into contact with a reference particle of known size. The center-to-center distance, d_c, of the two particle images, which was not affected by the image blur due to the diffraction limit, was measured as well as the broadened diameters of the reference and particle of interest, d_{ref} and d_1 affected by the diffraction broadening. The particle radius was calculated by using $r_1 = d_c/(1 + d_{ref}/d_1)$.[17] This has been demonstrated for microsphere sizes ranging from 3 μm and greater.

To illustrate the size distribution of the synthesized organosilica microspheres, imaging by Scanning Electron Microscopy (SEM) was employed. Samples were platinum coated and imaged using SEM (JEOL JSM 6400F) with accelerating voltage of 5 - 10 kV. The size distribution of the microspheres was obtained by processing the acquired images followed by statistical analysis.

2.2.2 Scattering Spectroscopy

In scattering spectroscopy, spherical particle extinction efficiency versus illumination wavelength (hereafter referred to as the scattering spectrum) was recorded. Recorded data were fitted to the theoretical model, where fitting parameters represented refractive index and size of the particle. The theoretical modelling would be straightforward if the experimental recording configuration was as simple as a plane wave incident on a single spherical non-absorbing particle that cast a shadow on a small-size photodetector situated at a distance. The attenuation of the incident optical flux along the axis of incidence would be entirely due to light scattering by the non-absorbing particle, or in other words, the particle scattered light away from the photodetector. Under typical experimental conditions, however, illumination from an extended light source could not be regarded as the plane wave illumination. In addition, instead of a single particle, one has to account for an ensemble of particles, and a finite photodetector size.

In this paper, we employed a commercial Lamda40 spectrophotometer (Perkin Elmer) to acquire sample extinction spectra. It should be noted that, generally, both scattering and

absorption contribute to the overall extinction spectra. However, in the wavelength range of our study scattering of our sample is significantly greater than absorption and the recorded scattering spectrum is representative of the extinction spectrum. The sample was an aqueous suspension of polystyrene or organosilica microspheres in a square-profile (10 mm × 10 mm) quartz cuvette. The concentration of the suspension was varied (average 1.5 ± 0.6 g/L) to ensure operation in the single-scattering regime without compromising the signal-to-noise ratio. Prior to spectroscopy session, every suspension was ultrasonicated for 3 minutes to ensure uniform suspension of microspheres. To verify suspension uniformity, spectrum measurements were repeated immediately after the first recording. In all cases spectra were identical, showing no effect of particle drift on the measurements. The cuvette was illuminated by a light source that produced a beam spot of approximately 1.0 × 7.5 mm^2 on the front facet of the cuvette, and was characterized by an angular divergence of 0.4° (see Fig. 1). A halogen lamp was used as the light source, in the visible and near-infrared spectral range, whereas a deuterium lamp was used in the ultraviolet spectral range. The illumination light source wavelength was selected by means of three spectrally adjacent tunable diffraction gratings whose operation wavelength range spanned 300 - 1100 nm. The detector was a silicon photodetector with an area of approximately 49 mm^2 calibrated for the wavelength range used. The source to detector configuration is shown in Fig. 1.

In addition, a cuvette with pure water was placed in the reference path of the spectrometer. Optical transmission spectra of the sample and reference were recorded over the wavelength range of 300 - 1100 nm, and each reference spectrum was subtracted

from the sample spectrum to account for reflections, aberrations and the intrinsic absorption profile of the solvent and cuvette material. Scans were performed at a rate of 480 nm min^{-1} with a spectral resolution of 2 nm. Recorded data were digitized and transferred to a personal computer for further processing, archiving, and display. The recorded data were fitted to the theoretical scattering spectra, as detailed in the modelling method in Section 3.

2.2.3 Laser Tweezers Refractometry

The second refractometry method is based on laser tweezers.[17, 18] Here, we measure the particle trapping potential created by a high-power focused laser beam, as shown in Fig. 2. For a particle displaced by a small distance, Δl, in transverse direction, the acting force, F_a, is measured. From this, the trap stiffness expressed in terms of the trap stiffness parameter, α, is calculated by $F_a/\Delta l$ (measured in piconewtons per nanometre, pN/nm). This stiffness was calculated for a particle of specified size for a range of refractive indices of the particle. From the theoretical analysis of measured results, as described in Section 3.2, we obtained the refractive index of microspheres. In order to create the optical particle trap, the beam from a continuous-wave fiber laser (power 1 watt, wavelength λ = 1070 nm) was focused to a diffraction-limited spot using an objective lens with high numerical aperture of 1.3. In order to detect a particle position in the beam, light from a helium-neon laser scattered by the particle was detected by using a quadrant photodetector. Alternatively, the fiber laser was used both for trapping and tracking of the particle position. In both cases, the particle displacement from the trap

centre generated a misbalanced photoelectrical signal on the photodetector quantifiable by means of the electronic signal processing. [19, 20]

3. Modelling method:

3.1 Scattering Spectroscopy

A typical scattering spectrum (see Fig. 3) exhibits three major features: ripples, local maxima, and a sloping curve. The ripple represents a small-contrast high-frequency sinusoidal signal superimposed on the large background signal. This ripple signal is the result of interference between the incident light and light internally reflected within the particle. It can provide an accurate measure of the product of microsphere diameter, D, and its refractive index, n_{sp}. It is important to note that the ripple signal is detectable only if the sample is monodisperse and the size parameter, $x = \pi D / \lambda$, is much greater than 1. Otherwise, the ripple structure of the signal is smeared and ultimately undetectable.[9, 21] The light source and detector configurations have little effect on the ripple structure of the scattering spectrum.

Local maxima (one which is marked by an arrow in Fig. 3.) can be explained by the Lorenz-Mie scattering theory. In brief, it is due to interference of the incident and diffracted light at the particle-medium interface. A phase delay acquired by the diffracted light depends on the particle diameter and its relative refractive index n_{sp} / n_m, where n_m is the refractive index of the medium. By thin film approximation and consideration of

the optical path length difference, the spectral separation between the maxima of the scattering spectrum curve can be determined:[11]

$$\Delta\lambda = (\lambda_{i+1} - \lambda_i) \approx \frac{\lambda_i^2}{D(n_{sp} - n_m)}, \qquad (1)$$

where *i* and *i +1* stand for the adjacent peaks wavelength indices. We note that the fidelity of this relationship is affected by the source-detector configuration. However, in the context of our work, it provides a good estimation of particle refractive index.

The sloping curve of the scattering spectrum is observable in Fig. 3 as tailing towards the long wavelength side. This sloping trend can be also explained in the Lorenz-Mie scattering theory framework. In brief, the optical scatter of a microsphere takes the form of scattering lobes. The larger the size parameter, *x*, the more pronounced and narrow its forward-scattering lobe. The shorter the wavelength of light incident on a sample of microspheres, the less power is scattered away from the photodetector, hence the greater intensity is detected. This consideration qualitatively explains the sloping trend of the recorded spectra, although accurate theoretical modelling is needed for precise fitting of experimental data to the theory, and is beyond the scope of this paper.

In order to obtain a dispersion curve for the refractive index, a Lorenz-Mie scattering model was used to calculate the extinction cross-section of monodisperse microspheres suspended in a homogeneous medium. These calculations assume an incident plane wave and a infinitesimally small-size far-field detector i.e. collection angle of zero.[22]

Refractive index dependence on the wavelength was described by the Cauchy dispersion relation. Its general form is given by

$$n(\lambda) = A + \frac{B}{\lambda^2} + \frac{C}{\lambda^4}, \qquad (2)$$

where the Cauchy coefficients A, B (μm^2) and C (μm^4) are unique to the material.[23] Using an unconstrained nonlinear optimization method implemented in Matlab, particle size and a dispersion curve of refractive indices over a wavelength range of 300 - 1100 nm were determined.

3.2 Optical tweezers refractometry

Optical tweezers refer to a technique of trapping a single microsphere immersed in fluid at the focus of a laser beam. It is well known that particles in fluid experience random Brownian motion. For a trapped microsphere, Brownian motion is suppressed, where the suppression efficiency is a monotonic function of the optical trap stiffness, α, which in turn depends on the microsphere size and refractive index. Therefore, the analysis of the Brownian motion amplitude versus the controllable stiffness provides a basis for the determination of the particle refractive index. The Brownian motion amplitude is determined by detecting the microsphere position fluctuation in the trap, which is analysed in terms of its power spectrum amplitude. The roll-off frequency f_0, of this spectrum provides a reliable measure of the trap stiffness via the following relationship:[17]

$$f_0 = \frac{\alpha}{2\pi\beta}, \qquad (3)$$

where β is the drag coefficient well tabulated for various fluids. α relates to x and n_{sp}. This dependence has been analysed in the framework of the generalized Lorenz-Mie theory and detailed elsewhere.[17, 24, 25] Experimental measurement of α and its comparison with the theoretical curve of α versus n_{sp} at a fixed x, yields the refractive index of the particle.

4. Results and Discussion

A low-dispersion particle sample is required for precise determination of refractive indices of microspheres by means of scattering spectroscopy. Fig. 4 shows a typical ensemble of organosilica microspheres imaged by SEM. The CV of organosilica microspheres was determined to be less than 10%, suitable for the scattering spectroscopy measurements.

Organosilica microspheres with well controlled diameters could be produced in the size range of 1 - 6 μm. In Fig. 5(a), (b), and (c), recorded and calculated spectra for 2.01 and 5.26 μm polystyrene and 5.94 μm organosilica microsphere samples, respectively, are presented. Large size organosilica microspheres were chosen to ensure the experimental spectra exhibited at least two maxima. In the case of the monodisperse 2.01 μm

polystyrene microsphere aqueous suspension sample, the recorded extinction spectra were accurately fitted by using the Lorenz-Mie theory. Results of the calculations of dispersion of polystyrene refractive index are presented in Fig. 6(a). The theoretical fitting curve was parameterized in terms of the Cauchy coefficients (presented in Table 1), which showed very good agreement with those reported in the literature. We believe that the good agreement between the experimental and theoretical data was due to the relatively small sphere size, which forward-scattered incident light over wide angles. The evaluation of the 2.01 μm polystyrene sphere scattering showed that the forward-scattering lobe overfilled the area of the photodetector for $\lambda > 390$ nm, as illustrated in the Fig. 5(a) inset. This qualitative model also explains the discrepancy between theoretical and experimental data at $\lambda < 390$ nm, where the next side-lobe incident on the detector interferes constructively with the original incident plane wave, unlike the forward-scattering lobe which interferes destructively, and accounts for the extinction in the forward direction. Therefore, the extinction is reduced in comparison with that calculated in the small photodetector approximation. Alternatively, one can view this in terms of the size parameter *x*. In Fig 5(a), the introduction of the second side-lobe can be observed at an *x*-value of 17. The effect of multiple side-lobe interference is much more pronounced in the case of the scattering spectrum of 5.26 μm polystyrene microspheres, shown in Fig. 5(b), and 5.94 μm organosilica microspheres, shown in Fig. 5(c). Here, the maximum *x*-values are 15 and 17. The insets of Fig. 5(a) and (b) illustrate the detection scenarios for 2.01 and 5.26 μm polystyrene sphere aqueous suspension, respectively. Obviously, reducing the detector size can avoid the collection of the side-scattering lobe.

However, commercially available spectrometers have relatively large size detectors, which are designed to maximize detection sensitivity.

Since the polystyrene microsphere sample was monodisperse, the ripple signal was readily detectable. However, exact fit of the recorded spectra cannot be obtained by straightforward fitting as this requires more complex calculations which account for the finite detector size. Alternatively, the ripple signal can be isolated from the sloping curve of the scattering spectra by applying a high-pass filter to the recorded spectra of polystyrene microspheres. The results are presented in Fig. 5(a′) and (b′) for 2.01 and 5.26 μm polystyrene microspheres, respectively. Cut-off frequencies were chosen such that local minima and maxima and ripple features were conserved. For the 5.26 μm polystyrene sample, we used the ripple signal to determine the refractive index dispersion relationship, provided an independent measurement of the particle size could be made. For the organosilica microspheres, the ripple structure was not observable due to relatively large CV value. Therefore, we used the local maxima to determine their refractive index. The maximum was isolated by high-pass filtering of the original spectra to suppress the sloping feature of the recorded spectrum. The resultant spectrum is shown in Fig. 5(c′), and displays a reasonable agreement with the theoretical scattering spectrum.

The Cauchy coefficients determined for polystyrene and organosilica microspheres are shown in Table 1, and illustrated as dispersion curves in Fig. 6. The dispersion curve and

coefficients for polystyrene microspheres[16] and fused silica are also included for comparison. It can be seen that there is a substantial difference in refractive indices of fused silica and organosilica, which is probably due to the high abundance of sulphur in organosilica resulting in the higher refractive index. Cauchy coefficients were found for sphere diameters of 1.96 and 5.26 μm for polystyrene, which agreed with manufacturer specifications (2.01 ± 0.05 μm). For organosilica microspheres, the average sphere diameter was found to be 6.02 μm, consistent with the slight swelling of the microbeads in water observed earlier. The uncertainty of these measurements are approximately 1.0%.

Multiple scattering was not accounted for in our modelling method. The effect of multiple scattering has been shown, in literature, to increase with optical depth (concentration) and gradually smoothes out the maxima and minima.[26] The spectra of solutions with increasing concentrations were recorded, and did not exhibit the effects of multiple scattering, which were observed in the work of Cohen [1975].[26]

The refractive index of the microspheres was also measured using optical tweezers refractometry. This method did not require monodisperse suspensions since only a single particle was measured at a time. For 2.09 μm polystyrene and 5.16 μm organosilica microspheres, the power spectrum amplitude of Brownian motion, shown in Fig. 7, was recorded, and the roll-off frequencies determined. Using Eq. (3) and tabulated drag constants, the trap stiffness was calculated, and is shown in Table 2. By using experimentally measured diameters of the trapped polystyrene and organosilica

microspheres we calculated α versus n_{sp} in the framework of the Lorenz-Mie scattering theory, with the results presented in Fig. 8. The intersection of the theoretical curves and corresponding horizontal lines of the determined values of α yielded the refractive index of the trapped microspheres. For polystyrene microspheres, we obtained a refractive index of n_{sp} = 1.58 ± 0.01 at λ = 1070 nm. This value deviates by a 0.6% from that given in literature.[16] For the organosilica microspheres, we obtained refractive indices of 1.52 ± 0.01 and 1.51 ± 0.01 at 589 and 1070 nm respectively, which were in a good agreement with the respective values of 1.518 and 1.511 obtained by the scattering spectroscopy method. For comparison with the scattering spectroscopy results, the refractive index values obtained by the laser tweezers refractometry are also shown in Fig. 6(a) and (b).

5. Conclusions

The refractive index of organosilica microspheres was determined in the 300 – 1100 nm wavelength range using the laser tweezers refractometry and scattering spectroscopy techniques. The refractive index of organosilica has been found to range from 1.60 - 1.51 over the wavelength range of 300 - 1100 nm, which is considerably greater than that of the organosilica substrate, fused silica. The development of the refractometry methods addressed in this paper can be useful for accurate determination of nano(micro)material refractive index *in situ*, whereas the tabulation of refractive index of organosilica microspheres has important applications to biological screening using flow cytometry.

Acknowledgements

We acknowledge the support of OzNano2Life, which is a project supported by the International Science Linkage program (CG060027). This work was also supported by the Australian Research Council (DP0451527 and FF0455861).

References

[1] C. R. Miller, R. Vogel, P. P. T. Surawski, S. R. Corrie, A. Ruhmann, and M. Trau, "Biomolecular screening with novel organosilica microspheres," Chemical Communications **38**, 4783-4785 (2005).

[2] C. R. Miller, R. Vogel, P. P. T. Surawski, K. S. Jack, S. R. Corrie, and M. Trau, "Functionalized organosilica microspheres via a novel emulsion-based route," Langmuir **21**, 9733-9740 (2005).

[3] A. van Blaaderen, and A. Vrij, "Synthesis and characterization of monodisperse colloidal organo-silica spheres," Journal of Colloid and Interface Science **156**, 1-18 (1993).

[4] F. Garcia-Santamaria, H. Miguez, M. Ibisate, F. Meseguer, and C. Lopez, "Refractive index properties of calcined silica submicrometer spheres," Langmuir **18**, 1942-1944 (2002).

[5] S. A. Alexandrov, A. V. Zvyagin, K. K. M. B. D. Silva, and D. D. Sampson, "Bifocal optical coherenc refractometry of turbid media," Optics Letters **28**, 117-119 (2003).

[6] Y. Colpin, A. Swan, A. V. Zvyagin, and T. Plakhotnik, "Imaging and sizing of diamond nanoparticles," Optics Letters **31**, 625-627 (2006).

[7] N. N. Boustany, S. C. Kuo, and N. V. Thakor, "Optical scatter imaging: subcellular morphometry in situ with Fourier filtering," Optics Letters **26**, 1063-1065 (2001).

[8] K. Chen, A. Kromin, M. P. Ulmer, B. W. Wessels, and V. Backman, "Nanoparticle sizing with a resolution beyond the diffraction limit using UV light scattering spectroscopy," Optics Communications **228**, 1-7 (2003).

[9] P. Chýlek, V. Ramaswamy, A. Ashkin, and J. M. Dziedzic, "Simultaneous determination of refractive-index and size of spherical dielectric particles from light-scattering data," Applied Optics **22**, 2302-2307 (1983).

[10] L. G. Guimaraes, and H. M. Nussenzveig, "Theory of Mie resonances and ripple fluctuations," Optics Communications **89**, 363-369 (1992).

[11] S. Scholz, R. Vacassy, J. Dutta, H. Hofmann, and M. Akinc, "Mie scattering effects from monodispersed ZnS nanospheres," Journal of Applied Physics **83**, 7860-7866 (1998).

[12] Y. Liu, X. Li, Y. L. Kim, and V. Backman, "Elastic backscattering spectroscopic microscopy," Opt. Lett. **30**, 2445-2447 (2005).

[13] C. E. Alupoaei, J. A. Olivares, and L. H. Garcia-Rubio, "Quantitative spectroscopy analysis of prokaryotic cells: vegetative cells and spores," Biosensors and Bioelectronics **19**, 893-903 (2004).

[14] M. R. Callahan, J. B. Rose, and L. Garcia-Rubio, "Use of multiwavelength transmission spectroscopy for the characterization of cryptosporidium parvum oocysts: quantitative interpretation," Environmental Science & Technology **37**, 5254-5261 (2003).

[15] Y. Mattley, G. Leparc, R. Potter, and L. Garcia-Rubio, "Light scattering and absorption model for the quantitative interpretation of human blood platelet spectral data," Photochemistry and Photobiology **71**, 610-619 (2000).

[16] X. Y. Ma, J. Q. Lu, R. S. Brock, K. M. Jacobs, P. Yang, and X. H. Hu, "Determination of complex refractive index of polystyrene microspheres from 370 to 1610 nm," Physics in Medicine and Biology **48**, 4165 - 4172 (2003).

[17] G. Knöner, S. Parkin, T. A. Nieminen, N. R. Heckenberg, and H. Rubinsztein-Dunlop, "Measurement of refractive index of single microparticles," Physical Review Letters **97**, 157402 (2006).

[18] A. Ashkin, J. M. Dziedzic, J. E. Bjorkholm, and S. Chu, "Observation of a single-beam gradient force optical trap for dielectric particles," Optics Letters **11**, 288-290 (1986).

[19] M. J. Lang, C. L. Asbury, J. W. Shaevitz, and S. M. Block, "An automated two-dimensional optical force clamp for single molecule studies," Biophysical Journal **83**, 491-501 (2002).

[20] G. Knöner, S. Parkin, N. R. Heckenberg, and H. Rubinsztein-Dunlop, "Characterization of optically driven fluid stress fields with optical tweezers," Physical Review. E **72**, 031507 (2005).

[21] P. Chýlek, and J. Zhan, "Interference structure of the Mie extinction cross section," Journal of the Optical Society America **6**, 1846-1851 (1989).

[22] H. C. van de Hulst, *Light scattering by small particles* (Wiley, New York, 1957).

[23] F. A. Jenkins, and H. E. White, *Fundamentals of optics* (McGraw-Hill, New York, 1976).

[24] T. A. Nieminen, N. R. Heckenberg, and H. Rubinsztein-Dunlop, "Computational modelling of optical tweezers," in *Optical trapping and optical micromanipulation*, K. Dholakia, and G. C. Spalding, eds. (2004), 514-523.

[25] T. A. Nieminen, H. Rubinsztein-Dunlop, and N. R. Heckenberg, "Multipole expansion of strongly focussed laser beams," Journal of Quantitative Spectroscopy and Radiative Transfer **79-80**, 1005-1017 (2003).

[26] A. Cohen, "Multiple scattering measurements as a function of wavelength by use of a dye laser," Applied Optics **14**, 268-269 (1975).

[27] I. H. Malitson, "Interspecimen comparison of the refractive index of fused silica," Journal of the Optical Society of America B **55**, 1205-1209 (1965).

Figures and Tables

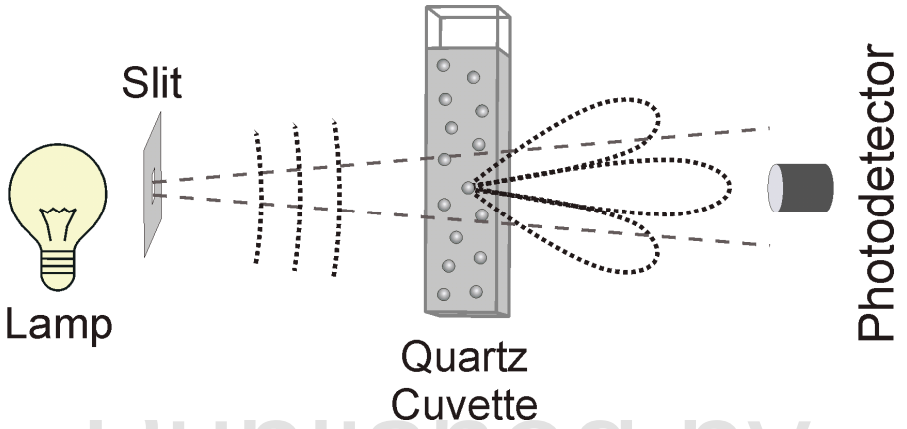

Fig. 1

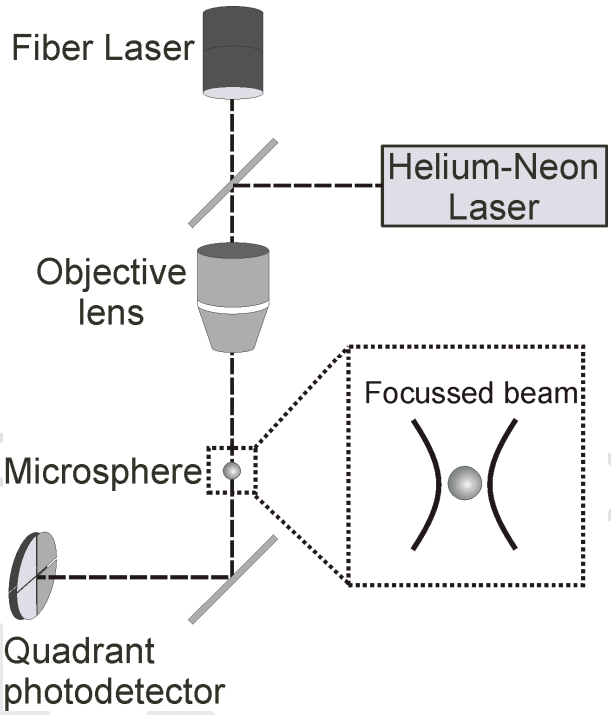
Fiber Laser
Helium-Neon Laser
Objective lens
Focussed beam
Microsphere
Quadrant photodetector

Fig. 2

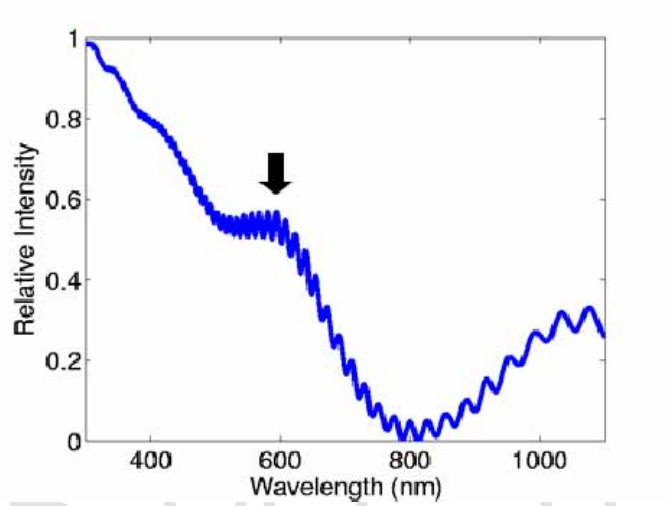

Fig. 3

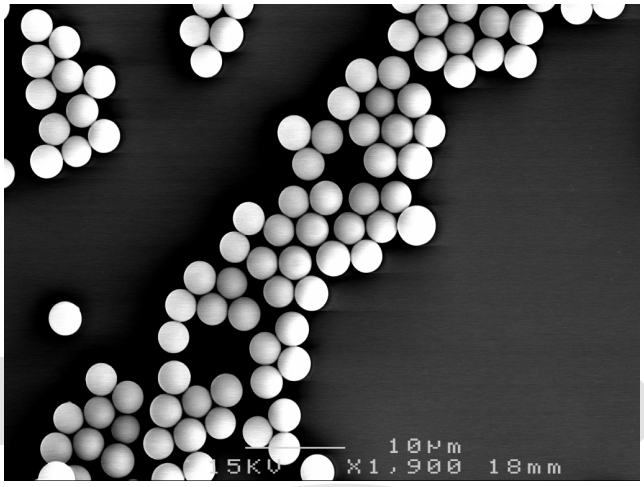

Fig. 4

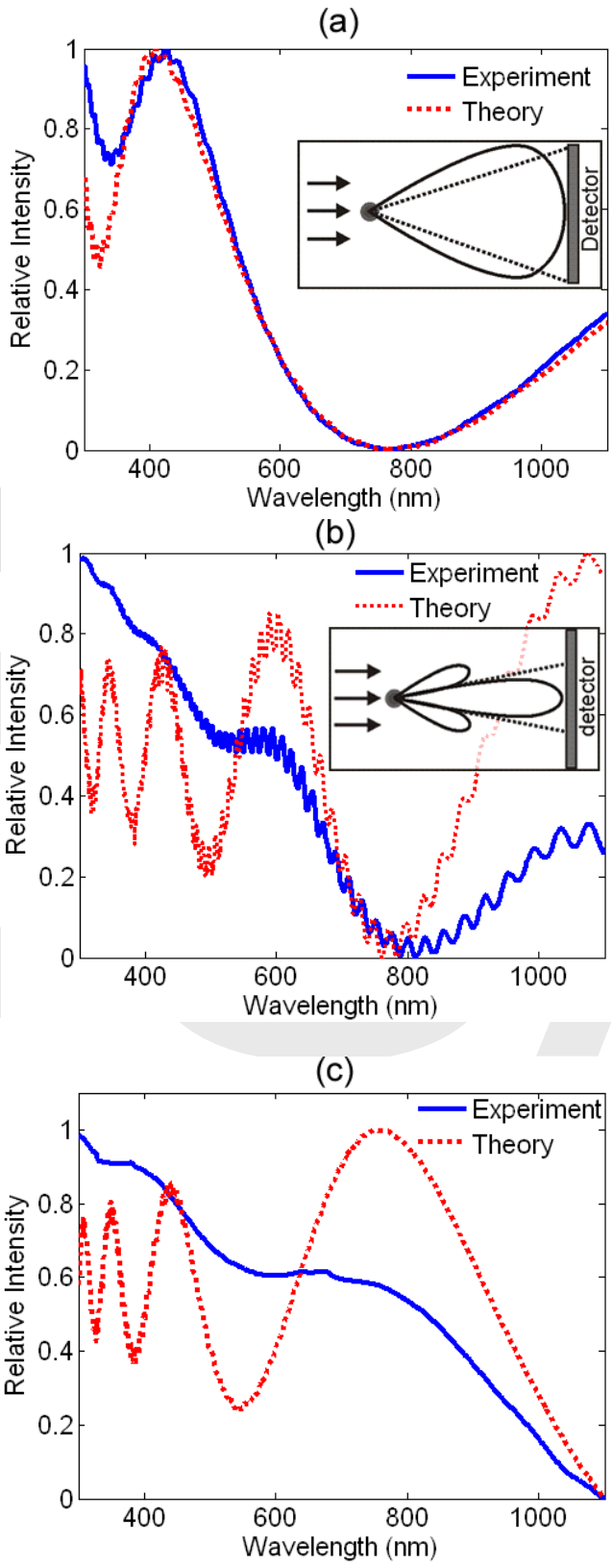
(a)
Experiment
Theory
Detector
Relative Intensity
Wavelength (nm)
(b)
Experiment
Theory
detector
Relative Intensity
Wavelength (nm)
(c)
Experiment
Theory
Relative Intensity
Wavelength (nm)

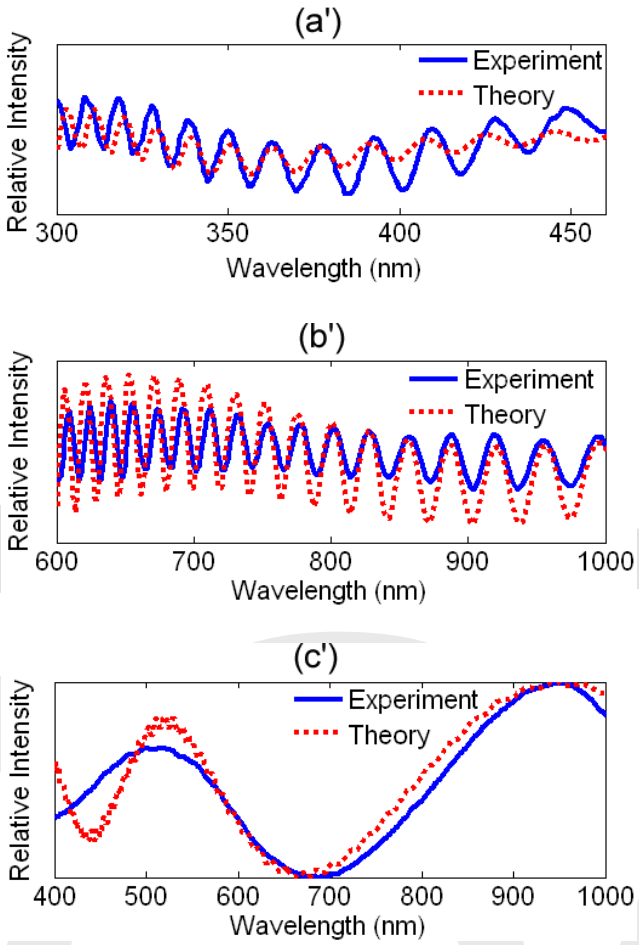
(a')
Relative Intensity
Experiment
Theory
300
350
400
450
Wavelength (nm)
(b')
Relative Intensity
Experiment
Theory
600
700
800
900
1000
Wavelength (nm)
(c')
Relative Intensity
Experiment
Theory
400
500
600
700
800
900
1000
Wavelength (nm)

Fig. 5

Table 1

	A	B ($\times 10^{-3}$ μm^{-2})	C ($\times 10^{-4}$ μm^{-4})	Wavelength λ (nm)
Ma *et al.* polystyrene[16]	1.5725	3.1080	3.4779	390-1310
2.01 μm polystryene	1.5865	-4.700	0.100	390-1100
5.26 μm polystyrene	1.5736	3.0499	4.0497	390-1100
Fused Silica[27]	1.4492	3.1200	0.3670	200-2000
Organosilica	1.5169	0.4231	6.6304	430-1100

Table 2

	f_o (Hz)	α (pN/nm)	β ($\times 10^{-9}$ pN/nm)
2.09 μm PS	2714	0.31	19.72
5.16 μm ogSI	383	0.117	48.6

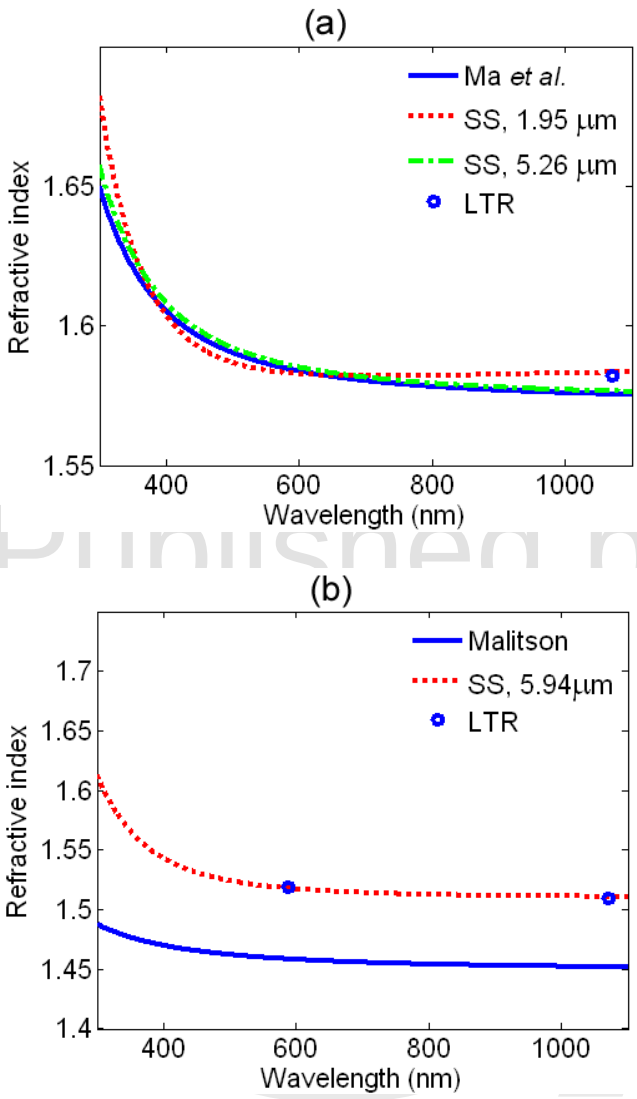
(a)
Ma et al.
SS, 1.95 μm
SS, 5.26 μm
LTR
Refractive index
1.65
1.6
1.55
400
600
800
1000
Wavelength (nm)
(b)
Malitson
SS, 5.94μm
LTR
Refractive index
1.7
1.65
1.6
1.55
1.5
1.45
1.4
400
600
800
1000
Wavelength (nm)

Fig. 6

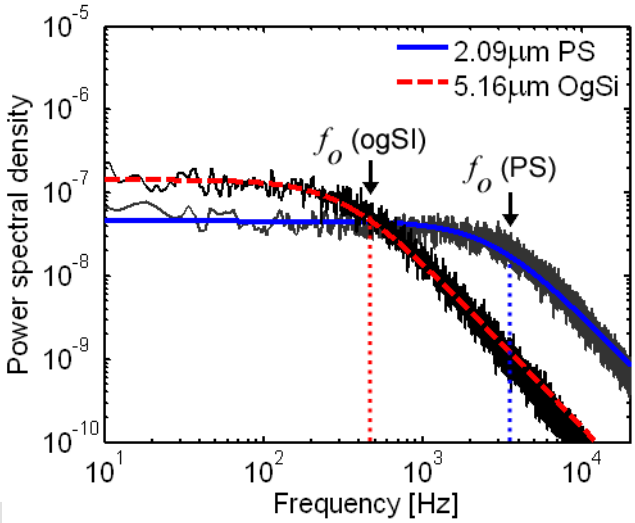

Fig. 7

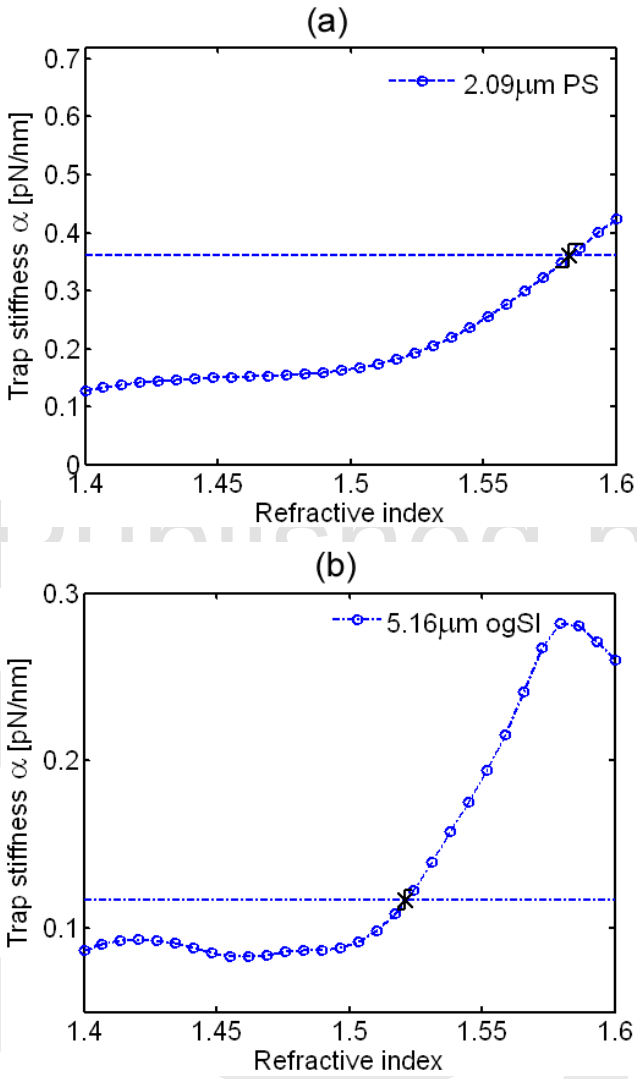
(a)
2.09μm PS
Trap stiffness α [pN/nm]
Refractive index
(b)
5.16μm ogSl
Trap stiffness α [pN/nm]
Refractive index

Fig. 8

Figure Captions

Fig. 1: A lamp emits a spherical wave of divergence of 0.4^{o} which is incident on a quartz cuvette filled with an aqueous suspension of microspheres. A single microsphere (not to scale), scatters the incident wave predominantly in the forward direction in a form of several lobes (pictured by dotted lines). A photodetector detects intensity of coherent superposition of transmitted and scattered light waves.

Fig. 2: Schematic diagram of the optical tweezers refractometry for refractive index measurement of individual microspheres. A microsphere was trapped by a tightly focused laser beam. The microsphere displacement from the center of the trap was detected by illuminating it with a helium-neon laser and detecting the signal on the quadrant photodetector. The inset shows the microsphere trapped at the center of the focussed fiber laser beam.

Fig. 3: Typical scattering spectrum of the microsphere suspension in solution. Three distinct features are observable: ripples, local maxima, and a sloping curve. An arrow points to the local maximum.

Fig. 4: SEM image of monodisperse organosilica microspheres.

Fig. 5: Recorded and calculated spectra of microsphere suspension of (a) 2.01 μm and (b) 5.26 μm, polystyrene and (c) 5.94 μm organosilica microspheres in water. Theoretcial spectra were obtained by optimization of Cauchy parameters. Insets illustrate the

detection scenarios for the microspheres in suspension. High-pass filtered spectra of (a′) 2.01 μm and (b′) 5.26 μm polystyrene, and (c′) 5.94 μm organosilica microsphere suspensions.

Fig. 6: (Color online) Refractive index dispersion of (a) polystyrene and (b) organosilica microspheres by scattering spectroscopy (SS) and laser tweezers refractometry (LTR). "Ma *et al*." denotes n_{sp} for polystyrene, as given by Ma *et al*. [2003][16]; "Malitson" denotes refractive index dispersion for fused silica, as given by Malitson [1965].[27]

Table 1: Cauchy coefficients for refractive index dispersion relation (Eq. 2)

Table 2: Parameters determined by Laser Tweezers Refractometry

Fig. 7: Plot of power spectral amplitude densities of 2.09 μm polystyrene (PS) and 5.16 μm organosilica microspheres (ogSI) versus frequency of particle Brownian motion in the optical tweezers trap. The roll-off frequency (f_o) was used to determine the trap stiffness.

Fig. 8: Theoretical plots of trap stiffness versus n_{sp} for (a) 2.09 μm polystyrene (PS), and (b) 5.16 μm organosilica microspheres (ogSI). The intersection of the theoretical curve and the measured trap stiffness (horizontal line) yields n_{sp}.